

# Engineering Notes

ENGINEERING NOTES are short manuscripts describing new developments or important results of a preliminary nature. These Notes cannot exceed 6 manuscript pages and 3 figures; a page of text may be substituted for a figure and vice versa. After informal review by the editors, they may be published within a few months of the date of receipt. Style requirements are the same as for regular contributions (see inside back cover).

## Calculation of Vortex Sheet Roll-up in a Rectangular Wind Tunnel

M. Mokry\*

National Research Council of Canada  
Ottawa, Canada

and

W. J. Rainbird†

Carleton University, Ottawa, Canada

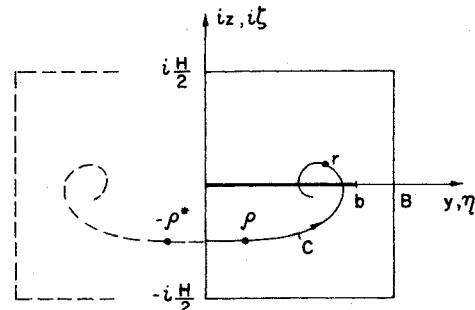


Fig. 1 Coordinate system.

THE possibility of calculating the roll-up of a vortex sheet wake in a rectangular wind tunnel with solid walls was earlier demonstrated by Hackett and Evans,<sup>1,2</sup> who represented the wind tunnel effect by a few layers of image vortex sheets. The present Note utilizes the more general concept of the influence (Green's) function, analogous to that used in Ref. 3. For simplicity, the method is applied to a vortex sheet in the time dependent  $y, z$  plane, proven by Betz<sup>4</sup> to preserve all essential features of the roll-up process, at least in the far field. The computations are performed by the discretization of the continuous vortex sheet model by finite length elements which show more stable behavior than Westwater's<sup>5</sup> array of point vortices. It appears from the present calculations that for a suitable distribution of vortex sheet elements and for appropriate time increments, the roll-up process can be followed over sufficiently large times without the need to introduce artificial viscosity<sup>6,7</sup> or smoothing.<sup>8</sup>

Assuming the wind-tunnel walls to be solid and the flow symmetrical about the  $z$ -axis, Fig. 1, we solve for the complex disturbance velocity  $w$  in the rectangle  $0 < y < B$ ,  $|z| < H/2$ , satisfying the boundary conditions

$$\operatorname{Re} w = 0 \quad y = 0, B \quad \operatorname{Im} w = 0 \quad z = \pm H/2 \quad (1)$$

By the principle of linear superposition  $w$  can be represented by the contour integral

$$w(r) = \int_C \gamma(\chi) g(r, \rho) d\chi \quad (2)$$

where

$$r = y + iz \quad (3)$$

$$\rho = \eta + i\xi \quad (4)$$

$C$  is the half of the vortex sheet and

$$d\chi = (d\eta^2 + d\xi^2)^{1/2} \quad (5)$$

its line element.

The real-valued function  $\gamma$  is the vortex density function (streamwise vorticity shed by the half wing). According to Prandtl's high-aspect ratio wing theory,  $\gamma$  relates to the spanwise distribution of bound circulation  $\Gamma$  through

$$\gamma(y) = d\Gamma(y)/dy \quad (6)$$

Load distributions satisfying  $\Gamma(y) = \Gamma(-y)$  and  $\Gamma(b) = 0$  where  $b$  is the span of the half wing, can be represented by the

Received January 14, 1975.

Index categories: Aircraft Aerodynamics (including Component Aerodynamics); Aircraft Testing (including Component Wind Tunnel Testing).

\*Associate Research Officer, NAE—High Speed Aerodynamics Laboratory. Member AIAA.

†Professor, Department of Mechanical and Aeronautical Engineering. Member AIAA.

series

$$\Gamma = b \sum_{n \in I} a_n \sin(n\theta) \quad (7)$$

where  $I$  is a set of odd natural numbers and

$$\theta = \arccos(y/b) \quad (8)$$

The influence function  $g$  can conveniently be written in the form

$$g(r, \rho) = f(r, \rho) + h(r, \rho) \quad (9)$$

The first term is the free air fundamental solution

$$f(r, \rho) = \frac{i}{2\pi} \left[ \frac{1}{r - \rho} - \frac{1}{r + \rho^*} \right] \quad (10)$$

which describes the complex disturbance velocity at the observation point  $r$  due to a pair of point vortices of strengths  $+1$  and  $-1$ , located at  $\rho$  and  $-\rho^*$ . (The asterisk indicates complex conjugation.) The second term  $h$  is an analytic function in the rectangle  $0 < y < B$ ,  $|z| < H/2$ , and represents the boundary effect of wind-tunnel walls.

For  $r \in C$ , indicating a point on the vortex sheet (tangential discontinuity), the integral of Eq. (2) is interpreted as the Cauchy principal value. Using the method of images,<sup>3</sup> the function  $g$  satisfying Eqs. (1, 9, and 10) is found to be

$$g(r, \rho) = \frac{i}{2H} \sum_{m=-\infty}^{\infty} \left\{ \exp \left[ \frac{\pi(r - \rho - 2mB)}{H} \right] - 1 \right\}^{-1} - \left\{ \exp \left[ \frac{\pi(r - \rho^* - 2mB)}{H} \right] + 1 \right\}^{-1} - \left\{ \exp \left[ \frac{\pi(r + \rho^* - 2mB)}{H} \right] - 1 \right\}^{-1} - \left\{ \exp \left[ \frac{\pi(r + \rho - 2mB)}{H} \right] + 1 \right\}^{-1} \quad (11)$$

The terms in braces represent the sums of singularities in the  $z$ -direction<sup>3</sup> so that we are left with only a single summation in the  $y$ -direction (horizontal reflections).

The numerical solutions are obtained by approximating the contour  $C$  by  $N$  straight-line elements. Denoting by  $r_j$  the mid-point of the  $j$ th element, and by  $\rho_j$  and  $\rho_{j+1}$  its end points we obtain

$$d\chi = d\rho(\rho_{j+1}^* - \rho_j^*) / |\rho_{j+1} - \rho_j| \\ = d\rho^*(\rho_{j+1} - \rho_j) / |\rho_{j+1} - \rho_j|$$

Assuming that over the  $j$ th element the functions  $\gamma$  and  $h$  have constant values  $\gamma_j$  and  $h(r_j, r_j)$ , respectively, and per-

Fig. 2 Time history of a vortex sheet roll-up,  $\Gamma/b = \sin \theta$ .

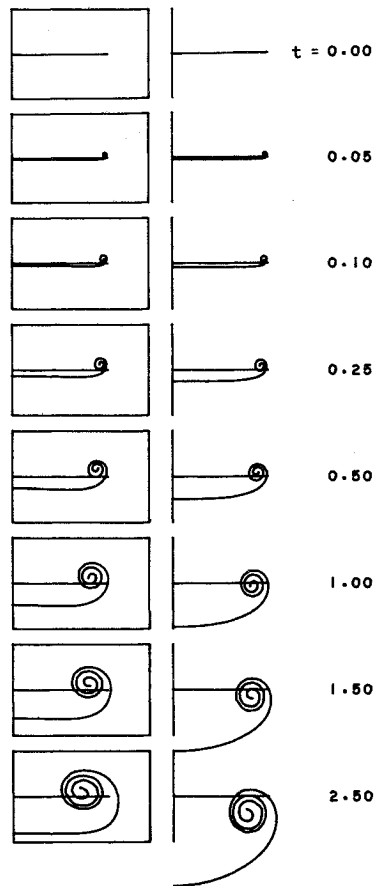
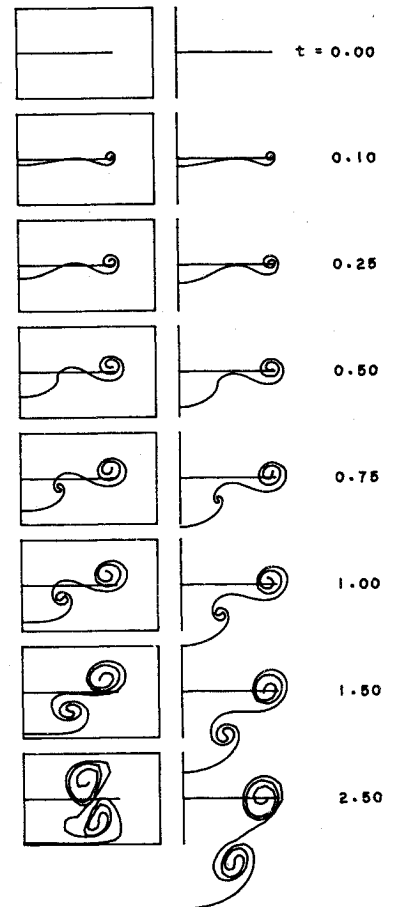


Fig. 3 Time history of a vortex sheet roll-up,  $\Gamma/b = \sin \theta + [(2)^{1/2}/10] \sin 5\theta$ .



forming the integration in Eq. (2) we obtain

$$w(r_k) = -\frac{i}{2\pi} \left\{ \gamma_k \frac{\rho_{k+1} - \rho_k}{|\rho_{k+1} - \rho_k|} \log \frac{r_k + \rho_{k+1}^*}{r_k + \rho_k^*} + \sum_{j=1, j \neq k}^N \gamma_j \left[ \frac{\rho_{j+1} - \rho_j}{|\rho_{j+1} - \rho_j|} \log \frac{r_k + \rho_{j+1}^*}{r_k + \rho_j^*} + \frac{\rho_{j+1}^* - \rho_j^*}{|\rho_{j+1} - \rho_j|} \log \frac{r_k - \rho_{j+1}}{r_k - \rho_j} \right] + \sum_{j=1}^N \gamma_j |\rho_{j+1} - \rho_j| h(r_k, r_j) \right\} \quad (12)$$

Denoting by superscripts  $s$  the coordinates in the  $s$ th time step, the following scheme is adopted<sup>†</sup>

$$\rho_{k+1}^{s+1} = \rho_{k+1}^s + 1/2 [w(r_{k+1}^s) + w(r_k^s)] * \Delta t^s \quad (13)$$

$$r_{k+1}^{s+1} = 1/2 (\rho_{k+1}^{s+1} + \rho_k^{s+1}) \quad (14)$$

where  $\Delta t^s$  is the time increment in the  $s+1$ th time step.

By the law of conservation of vorticity

$$\gamma_k^{s+1} = \gamma_k^s |\rho_{k+1}^s - \rho_k^s| / |\rho_{k+1}^{s+1} - \rho_k^{s+1}| \quad (15)$$

To save in computation time, the time increment is adjusted according to

$$\Delta t^{s+1} = \Delta t^s \max_k |\gamma_k^s| / \max_k |\gamma_k^{s+1}| \quad (16)$$

Examples calculated by the presently described method are exhibited in Figs. 2 and 3. Vortex roll-up histories in free air

<sup>†</sup>In Sept. 1975 the authors learned from P. T. Fink of the University of New South Wales, Australia, of the "stepwise vorticity discretization method" which is similar to the present approach.<sup>12</sup>

are compared with those in a solid wall wind tunnel for the following case:  $B/b = 1.43$ ,  $H/b = 0.95$ . This corresponds to related experiments being currently conducted at the Carleton University low-speed wind tunnel.

Figure 2 shows results for an elliptic load distribution,  $\Gamma/b = \sin \theta$  using 50 elements distributed according to  $\rho_k^0/b = \sin [(\pi/2)(k-1)/50]$ , and choosing  $\Delta t^0 = 0.0005$ . To reach the "time"  $t = 2.5$ , 100 time steps were required in each case. With the exception of the downwash, the roll-up patterns seem to differ very little in the initial stage. Later, however, the wind-tunnel spiral tends to deform (flatten in this case) according to the constraining walls.

The wind-tunnel distortion effect is more pronounced in Fig. 3, obtained for the load distribution  $\Gamma/b = \sin \theta + [(2)^{1/2}/10] \sin 5\theta$  (10% induced drag penalty). The function  $|\gamma|$  has a local minimum at  $y/b \approx 0.78$ , and as predicted by Donaldson et al.<sup>10</sup> and Yates,<sup>11</sup> a double roll-up vortex is developed. The computations are performed using 75 elements,  $\rho_k^0/b = \sin [(\pi/2)(1.01^{k-1} - 1)/(1.01^{75} - 1)]$ , and choosing again  $\Delta t^0 = 0.0005$ . In this case 80 time steps were needed to reach  $t = 2.5$ .

Analysis of the data obtained confirms a significant feature of the vortex sheet roll-up in a closed-wall wind tunnel, namely that the vorticity distribution has essentially a stationary center of gravity. This is in marked contrast with the free air case where the center of gravity, while preserving its spanwise coordinate, moves downwards (negative  $z$ -direction).

## References

- Hackett, J. E. and Evans, M. R., "Simplified Image Systems for the Simulation of Rectangular Wind Tunnels," ER-10114, June 1969, Lockheed-Georgia Co., Marietta, Ga.
- Hackett, J. E. and Evans, M. R., "Vortex Wakes Behind High-Lift Wings," *Journal of Aircraft*, Vol. 8, May 1971, pp. 334-340.

<sup>3</sup>Mokry, M., "Integral Equation Method for Subsonic Flow past Airfoils in a Ventilated Wind Tunnel," *AIAA Journal*, Vol. 13, Jan. 1975, pp. 47-53.

<sup>4</sup>Betz, A., "Verhalten von Wirbelsystemen," *Zeitschrift für angewandte Mathematik und Mechanik*, Vol. 12, 1932, pp. 164-174.

<sup>5</sup>Westwater, F. L., "The Rolling Up of the Surface of Discontinuity behind an Aerofoil of Finite Span," *R&M* 1692, Aug. 1935, Aeronautical Research Council, London, Eng.

<sup>6</sup>Kuwahara, K. and Takami, H., "Numerical Studies of Two-Dimensional Vortex Motion by a System of Point Vortices," *Journal of the Physical Society of Japan*, Vol. 34, Jan. 1973, pp. 247-253.

<sup>7</sup>Bloom, A. M. and Jen, H., "Roll-Up of Aircraft Trailing Vortices using Artificial Viscosity," *Journal of Aircraft*, Vol. 11, Nov. 1974, pp. 714-716.

<sup>8</sup>Chorin, A. J. and Bernard, P. S., "Discretization of a Vortex Sheet, with an Example of Roll-Up," *Journal of Computational Physics*, Vol. 13, Nov. 1973, pp. 423-429.

<sup>9</sup>Clements, R. R. and Maull, D. J., "The Rolling Up of a Trailing Vortex Sheet," *Aeronautical Journal*, Vol. 77, Jan. 1973, pp. 46-51.

<sup>10</sup>Donaldson, C. duP., Snedeker, R. S., and Sullivan, R. D., "Calculation of Aircraft Wake Velocity Profiles and Comparison with Experimental Measurements," *Journal of Aircraft*, Vol. 11, Sept. 1974, pp. 547-555.

<sup>11</sup>Yates, J. E., "Calculation of Initial Vortex Roll-up in Aircraft Wakes," *Journal of Aircraft*, Vol. 11, July 1974, pp. 397-340.

<sup>12</sup>Fink, P. T. and Soh, W. K., "Calculation of Vortex Sheets in Unsteady Flow and Applications in Ship Hydrodynamics," Proceedings of Tenth Symposium on Naval Hydrodynamics, M.I.T., Cambridge, Mass., June 1974.

## Effect of Compression Ratio on NO<sub>x</sub> Production by Gas Turbines

J. L. Kerrebrock\*

Massachusetts Institute of Technology,  
Cambridge, Mass.

IT is well established as a result of correlations by Lipfert,<sup>1</sup> supported by Bahr<sup>2</sup> and by Nelson,<sup>3</sup> that the mass fraction of NO<sub>x</sub> in the exhaust gases of currently operational aircraft gas turbines increases dramatically with compressor outlet temperature, hence with compression ratio. Sawyer et al.<sup>4</sup> and Ferri and Agnone<sup>5</sup> prefer a correlation in terms of maximum combustion temperature, but for the rather narrow range of equivalence ratios in the primary zones of existing combustors these correlations appear to be essentially equivalent.

The purpose of this Note is to point out that these correlations do not necessarily imply that a higher NO<sub>x</sub> fraction in the exhaust must be accepted as a result of increased compression ratio and turbine inlet temperature, even for currently available burner technology.

As Lipfert<sup>1</sup> and Sawyer et al.<sup>4</sup> point out, the data correlations imply near constancy of the residence times in the primary zones of the burners for the engines correlated. The dramatic rise in NO<sub>x</sub> with increasing compressor outlet temperature then follows from an increase in the rate of NO<sub>x</sub> formation roughly according to the relation

$$(\text{NO}_x) \propto p_3^{1/2} e^{-2400/T_3 \tau_p}$$

where  $p_3$  and  $T_3$  are compressor outlet pressure and temperature and  $\tau_p$  is the residence time in the primary zone.

Note, however, that since the rates of the combustion reactions also are increased as  $T_3$  and  $p_3$  increase, it should be

Received March 25, 1975.

Index categories: Reactive Flows; Combustion in Gases; Thermochemistry and Chemical Kinetics.

\*Professor, Department of Aeronautics and Astronautics; also Director, Gas Turbine Laboratory. Fellow AIAA.

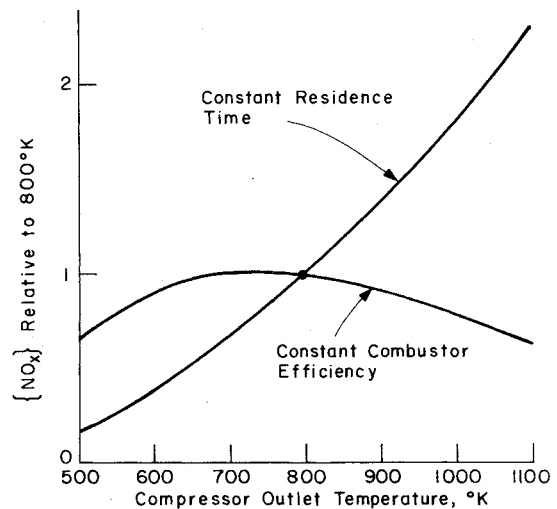


Fig. 1 Comparison of the variations of NO<sub>x</sub> mass fraction with compressor outlet temperature which should result for burners having constant combustion efficiency, with that for burners having constant primary zone residence time.

possible to decrease  $\tau_p$  as  $T_3$  and  $p_3$  are increased. Indeed, correlations of combustor efficiency,  $\eta_b$ , for fixed geometry combustors have indicated a correlation of the form<sup>6</sup>

$$\eta_b(p_3^{1.75} e^{T_3/b}/m)$$

where  $m$  is mass flow through the burner, and  $b$  varies from 300 K for a fuel air ratio of 0.016 to 150K for 0.010. Taking  $\tau_p \propto p_3/m$ , i.e., neglecting small temperature changes in the primary zone, and assuming  $p_3 \propto T_3^{(\gamma-1)/\gamma}$  we find that for constant combustion efficiency

$$(\text{NO}_x) \propto e^{-[(2400/T_3) + (T_3/b)]/T_3^{0.25\gamma/(\gamma-1)}} (\eta_b = \text{constant})$$

This result is plotted in Fig. 1, compared to the corresponding result for  $\tau_p = \text{constant}$ . We see that the NO<sub>x</sub> mass fraction is sensibly constant over the range of  $T_3$  from 600 to 900K, and is even predicted to fall off at higher compressor outlet temperatures. Hence the conclusion that for constant combustion efficiency in a given combustor design, NO<sub>x</sub> is nearly independent of combustor inlet temperature.

The author is aware that the requirement for low CO and hydrocarbon efflux at part throttle conditions dictates high combustion efficiency at these conditions, and that combustion efficiency tends to decrease with decreased throttle setting for fixed geometry combustors. The part throttle requirements can be and have been met with fixed geometry combustors by choosing residence times longer than are required for full power operation. This solution is attractive in part because combustor length and volume are not as critical in large high pressure ratio engines as they were in early small turbojets.

It is suggested therefore, that NO<sub>x</sub> production in high-pressure ratio engines can be reduced by designing for the minimum primary zone residence time consistent with combustion efficiency at full power, and then achieving satisfactory part throttle combustion efficiency by some scheme such as compressor outlet bleed or combustor bypass.

## References

- <sup>1</sup>Lipfert, F. W., "Correlation of Gas Turbine Emissions Data," ASME Paper 72-GT-60, March 1972.
- <sup>2</sup>Bahr, D. W., "Technology for the Reduction of Aircraft Turbine Engine Exhaust Emissions," *Atmospheric Pollution by Aircraft Engines*, AGARD-CP-125, April 1973.
- <sup>3</sup>Nelson, A. W., "Detailed Exhaust Emissions Measurements of Three Different Turbofan Engine Designs," AGARD-CP-125, April 1973.